Sound & Vibration 2025, 59(1), 1839.
https://doi.org/10.59400/sv1839

Article

Clear imaging beamforming method for the noise source identification in car cabin

Yuping Wan[1], Jinfeng Xia[1], Liang Yang[1], Yang Yang[2,*], Zhigang Chu[3,*]

[1] State Key Laboratory of Intelligent Vehicle Safety Technology, Chongqing ChangAn Automobile Co., Ltd., Chongqing 401133, China
[2] Chongqing Automotive Power System Testing Engineering Technology Research Center, School of Vehicles Engineering, Chongqing Industry Polytechnic College, Chongqing 401120, China
[3] College of Mechanical and Vehicle Engineering, Chongqing University, Chongqing 400044, China
*** Corresponding authors:** Yang Yang, yangyang@cqipc.edu.cn; Zhigang Chu, zgchu@cqu.edu.cn

CITATION

Wan Y, Xia J, Yang L, et al. Clear imaging beamforming method for the noise source identification in car cabin. Sound & Vibration. 2025; 59(1): 1839. https://doi.org/10.59400/sv1839

ARTICLE INFO

Received: 9 October 2024
Accepted: 22 October 2024
Available online: 22 November 2024

Abstract: Noise in car cabin has a close relationship with ride comfort and noise control plays a key role in automobile product design. The prerequisite of noise control is to accurately identify noise sources. Due to the advantages of recording comprehensive sound field information and achieving panoramic source identification, beamforming with spherical microphone array is suitable for interior sound source identification. However, classic spherical harmonics beamforming (SHB) and filter and sum (FAS) suffer from wide mainlobes and serious sidelobe contamination. This paper proposes clear imaging beamforming method, which repeatedly removes the independent contribution of each source from SHB output based on coherence between sidelobe and mainlobe to improve imaging clarity. Simulations and experiments demonstrate that the proposed method has much clearer imaging than SHB and FAS, and could effectively identify the noise sources in car cabin.

Keywords: noise control in car cabin; noise source identification; beamforming; spherical microphone array; clear imaging

1. Introduction

The noise in car cabin has a close relationship with ride comfort and plays a key role when evaluating the index, and noise also adversely affects the mental and physical health of humans [1–3]. To develop the automobile market economy and improve health, it is vital to control noise and improve sound quality inside car cabin during the automobile product design. The most primary and the most effective method for noise control and sound quality improvement is to control noise source, i.e., employ indoor noise source identification technology to accurately localize noise source, obtain its frequency and quantify its strength, and then take the corresponding measures to reduce noise.

Due to the capability of recording comprehensive sound field information and the advantage of achieving panoramic source identification, beamforming with spherical microphone array has attracted much attention in the field of interior sound source identification in recent years [4–7]. Spherical harmonics beamforming (SHB) [8–10] is the most common beamforming algorithm using spherical microphone array, which utilizes the orthogonality of spherical harmonics to form mainlobes at the position of the true sources and sidelobes at other positions. SHB possesses high robustness and high efficiency, however, it suffers from wide mainlobes and serious sidelobe contamination [11–13]. It is worth mentioning that car cabin noise typically peaks at

low frequencies (below 500 Hz), thus SHB will shows much wider mainlobes, which adversely affects source identification.

To improve the clarity, many researchers make efforts. Koretz et al. [14] proposed a Dolph-Chebyshev beampattern design method for SHB to yield an expected mainlobe width or maximum dynamic range. Yan et al. [15] established a spherical harmonics-based minimum variance distortionless response beamformer which could minimize sidelobe peaks and keep distortionless response in look directions at the same time. Hald [16] developed a filter and sum (FAS) beamforming method, which achieves dynamic range enhancement by establishing a second order cone program model. Tiana-Roig et al. [17] tried to use acoustic holography to improve spatial resolution at low frequencies. However, these solutions still cannot provide sufficiently clear and unambiguous imaging for sources. Hence, this paper proposes clear imaging beamforming method for noise source identification in car cabin, which repeatedly removes the independent contribution of each source from SHB output based on coherence between sidelobe and mainlobe to improve imaging clarity. The remainder of this paper is organized as follows: Section 2 elaborates the theory of the proposed method, Section 3 investigates the performance of the proposed method via simulations and experiments, and Section 4 summarizes the conclusions.

2. Theory

Since the paper focuses on the noise source identification in car cabin, we establish a near-field measurement model, where source emits spherical waves. **Figure 1** shows the measurement model and a spherical coordinate system, where the symbols "⊙" and " • " represent sound source and microphones. An arbitrary point in the coordinate system is described as $(r,\ \Omega)$, r is the distance between the point and the origin, and $\Omega = (\theta,\ \phi)$ denotes the direction of the point, θ ($\theta \in [0,\ 180°]$) is the elevation angle, and ϕ ($\phi \in [0,\ 360°)$) is the azimuth angle. The position of the i th ($i = 1,\ 2,\ \cdots,\ I$) source and the q th ($q = 1,\ 2,\ \cdots,\ Q$) microphone is written as $(r_{S_i},\ \Omega_{S_i})$ and $(a,\ \Omega_{M_q})$, respectively. I and Q are the number of sources and microphones. a denotes the radius of spherical microphone array.

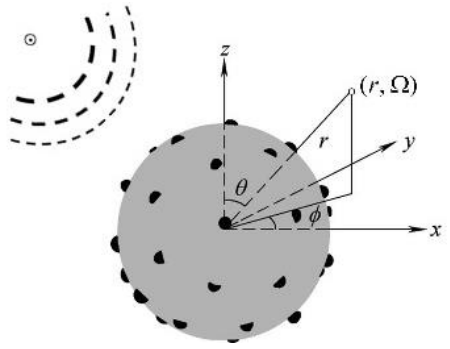

Figure 1. Spherical coordinate system and spherical microphone array.

We let the sampled pressure be $p \in \mathbb{C}^{Q\times 1}$, and the cross-spectrum matrix (CSM) be $C = \mathbb{E}(pp^H)$, where $\mathbb{E}(\cdot)$denotes the expectation and the superscript "H" represents Hermitian transpose. We firstly discretize the entire focus sphere into a set of grid

points, and each point is expressed as $(kr_{F_g},\ \Omega_{F_g})$ $g = 1,\ 2,\ \cdots,\ G$ is the index of points, and G is the number of grid points. According to [10], the output at each grid point of SHB is

$$b(kr_{F_g},\ \Omega_{F_g}) = u^H(kr_{F_g},\ \Omega_{F_g})Cu(kr_{F_g},\ \Omega_{F_g}) \tag{1}$$

where $u(kr_{F_g},\ \Omega_{F_g}) = \left(\frac{4\pi e^{ikr_{F_g}}}{(N+1)^2 kr_{F_g}}\right)\Gamma Y_{MN}(B_{FN}^{-1})^H y_{FN}^H$ is the sound pressure weight vector, k is the wave number, $i = \sqrt{-1}$ is the imaginary unit, $\Gamma = \mathrm{diag}(w)$, $\mathrm{diag}(\cdot)$ constructs a diagonal matrix which takes the vector in parentheses as diagonal, $w = [w_1,\ w_2,\ \cdots,\ w_Q]^T \in \mathbb{R}^{Q\times 1}$ is microphone weight vector. $y_{FN} \equiv y_N(\Omega_{F_g}) = \{\underbrace{Y_0^0(\Omega_{F_g})}_{n=0}\ \underbrace{Y_1^{-1}(\Omega_{F_g})\quad Y_1^0(\Omega_{F_g})\quad Y_1^1(\Omega_{F_g})}_{n=1}\ \cdots\ \underbrace{Y_N^{-N}(\Omega_{F_g})\quad \cdots\quad Y_1^N(\Omega_{F_g})}_{n=N}\} \in \mathbb{C}^{1\times(N+1)^2}$ is the spherical harmonics function vector, $Y_{MN} = \left[(y_{M_1N})^T,\ (y_{M_2N})^T,\ \cdots,\ (y_{M_QN})^T\right]^T = [y_N(\Omega_{M_1})^T,\ y_N(\Omega_{M_2})^T,\ \cdots,\ y_N(\Omega_{M_Q})^T]^T \in \mathbb{C}^{Q\times(N+1)^2}$ is the spherical harmonics function matrix, $Y_n^m(\Omega)$ is the spherical harmonics in the direction of Ω with the order of n and the degree of m. $B_{FN} = \mathrm{diag}([\underbrace{b_0(kr_F,\ ka)}_{n=0}\ \underbrace{b_1(kr_F, ka)\, b_1(kr_F, ka)\, b_1(kr_F, ka)}_{n=1}\cdots\underbrace{b_N(kr_F, ka)\cdots b_N(kr_F, ka)}_{n=N}]) \in \mathbb{C}^{(N+1)^2\times(N+1)^2}$ is the mode strength matrix, $b_n(kr_F, ka)$ is the mode strength with the order of n.

The core idea of clear imaging beamforming is to rewrite the output of SHB as a sum of contribution of each incoherent source and repeatedly remove the independent output of each source from SHB output based on coherence between sidelobe and mainlobe to achieve source identification. The steps are as follows: The degraded CSM is initialized to $D^{(0)} = C \in \mathbb{C}^{Q\times Q}$, the output of clear imaging beamforming is initialized to $P_C^{(0)} = 0 \in \mathbb{R}^{Q\times Q}$, and the residual matrix is initialized to $b^{(0)} = [b(kr_{F_g},\ \Omega_{F_g})|g = 1,\ 2,\ \cdots,\ G]$. At the $(\gamma+1)$ th iteration, we define the maximum output as $b_{max}^{(\gamma+1)}max^{(\gamma)}$, and $\Omega_{\max}^{(\gamma+1)}$ is the direction of the grid point corresponding to $b_{max}^{(\gamma+1)}$. Then, we use the peak of SHB output as the output of clear imaging beamforming, i.e.,

$$P_C^{(\gamma+1)} = P_C^{(\gamma)} + \vartheta b_{max}^{(\gamma+1)} \tag{2}$$

where ϑ is the loop gain used to control mainlobe width and Ψ is a matrix composed by Kronecker delta function $\delta_{\Omega_{F_g}}$. When $\Omega_{F_g} = \Omega_{max}^{(\gamma+1)}$, $\delta = 1$, otherwise, $\delta = 0$. Equation (2) indicates that the direction corresponding to the peak of output is where the strongest source locates in the current iteration.

We define a source component vector $\boldsymbol{s}(kr_{\max}^{(\gamma+1)}, \Omega_{\max}^{(\gamma+1)}) \in \mathbb{C}^{Q\times 1}$ to represent the CSM of the identified source in this iteration,

$$\boldsymbol{G}^{(\gamma+1)} = b_{\max}^{(\gamma+1)}\boldsymbol{s}(kr_{\max}^{(\gamma+1)}, \Omega_{\max}^{(\gamma+1)})\boldsymbol{s}^H(kr_{\max}^{(\gamma+1)}, \Omega_{\max}^{(\gamma+1)}) \tag{3}$$

The coherence between the maximum beamforming output and the output at an arbitrary point is

$$\boldsymbol{u}^H(kr_{F_g}, \Omega_{F_g})\boldsymbol{D}^{(\gamma)}\boldsymbol{u}(kr_{\max}^{(\gamma+1)}, \Omega_{\max}^{(\gamma+1)}) = \boldsymbol{u}^H(kr_{F_g}, \Omega_{F_g})\boldsymbol{G}^{(\gamma+1)}\boldsymbol{u}(kr_{\max}^{(\gamma+1)}, \Omega_{\max}^{(\gamma+1)}) \tag{4}$$

The reason why the equality in Equation (4) holds is that the maximum output is only contributed by the identified source. Combining Equations (3) and (4),

$$\boldsymbol{s}(kr_{\max}^{(\gamma+1)}, \Omega_{\max}^{(\gamma+1)}) = \frac{1}{b_{\max}^{(\gamma+1)}}\boldsymbol{D}^{(\gamma)}\boldsymbol{u}(kr_{\max}^{(\gamma+1)}, \Omega_{\max}^{(\gamma+1)}) \tag{5}$$

Remove $G_{\square}^{(\gamma+1)}$ from the current total CSM,

$$\boldsymbol{D}^{(\gamma+1)} = \boldsymbol{D}^{(\gamma)} - \vartheta b_{\max}^{(\gamma+1)}\boldsymbol{s}(kr_{\max}^{(\gamma+1)}, \Omega_{\max}^{(\gamma+1)})\boldsymbol{s}^H(kr_{\max}^{(\gamma+1)}, \Omega_{\max}^{(\gamma+1)}) \tag{6}$$

and then update SHB output at the point Ω_{F_g} according to Equation (7) to remove the contribution of the identified source to prepare for the next iteration,

$$b(kr_{F_g},\ \Omega_{F_g})^{(\gamma+1)} = u^H(kr_{F_g},\ \Omega_{F_g})D^{(\gamma+1)}u(kr_{F_g},\ \Omega_{F_g}) \tag{7}$$

The iteration stops when

$$\sum_{q_1=1}^{Q}\sum_{q_2=1}^{Q}\left|D^{(\gamma+1)}(q_1,\ q_2)\right| \geq \sum_{q_1=1}^{Q}\sum_{q_2=1}^{Q}\left|D^{(\gamma)}(q_1,\ q_2)\right| \tag{8}$$

where $D^{(\gamma)}(q_1,\ q_2)$ is the element in the q_1 th row and q_2 th column of $D^{(\gamma)}$.

3. Simulation and experiment

We first conduct simulations using a 36-channel rigid spherical microphone array. The radius of the array is 0.0975 m. Two sources at 500 Hz located at (1 m, 90°, 100°) and (1 m, 90°, 280°) are assumed. Their strengths are both 100 dB. The number of snapshot is set to 30. **Figure 2** shows the contour maps processed by SHB, FAS, clear imaging beamforming at three different SNRs (40 dB, 20 dB, and 10 dB). By comparing these maps, we can find: SHB and FAS suffer from wide mainlobes. Compared with SHB and FAS, the proposed method shows much clearer imaging with narrower mainlobes and no sidelobe contamination. Even at lower SNRs, the localization error of clear imaging beamforming is still 0, and this method shows better performance than SHB and FAS, indicating it is robust to noise interference. To obtain **Figure 2a**,**d**,**g**, SHB, FAS and clear imaging beamforming require 1.55 s, 12,600 s, and 1.55 s, respectively, which indicates the computational efficiency of clear imaging beamforming is comparable to SHB, significantly higher than FAS. It should be noted that the reason why FAS is so time-consuming is that it needs to calculate weighting vectors.

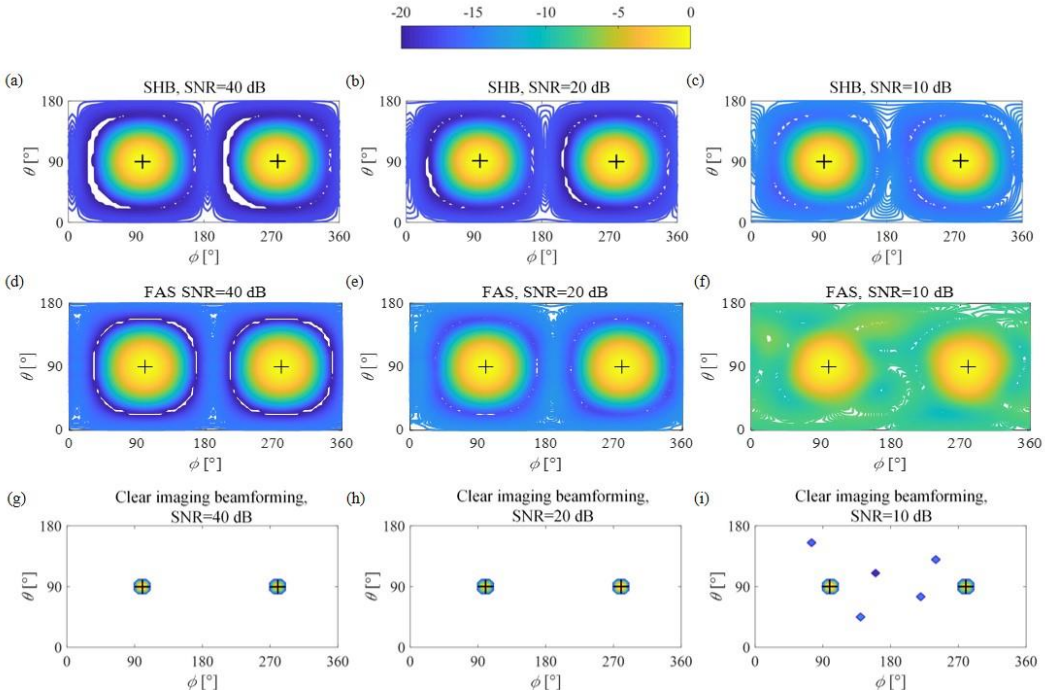

Figure 2. Contour maps of SHB and clear imaging beamforming.

We use SHB, FAS and clear imaging beamforming to identify noise in the cabin of an electric vehicle at the speed of 60 km/h. The layout is shown in **Figure 3**. We employ BK Type 8608 36-channel rigid spherical microphone array and BK Type 3660C data acquisition system to sample pressure signal, then apply FFT to the sampled signals in BKConnect software. The sampling frequency is 16,384 Hz, and the length of measurement time is 5 s. Each snapshot has a length of 500 ms, with Hanning window weighting, corresponding to a frequency resolution of 2 Hz. The overlap of two consecutive snapshots is set to 50%. The experimental results are shown in **Figure 4**. From those maps, we could find that clear imaging beamforming shows narrower mainlobes than SHB and FAS and indicates that the main noise source at 216 Hz is located at left rear door. We add weight to the door as shown in **Figure 4d** and we see an obvious decrease in the amplitude at 216 Hz in **Figure 4e**, which shows the proposed method effectively locates the noise sources in the electric vehicle at the frequency.

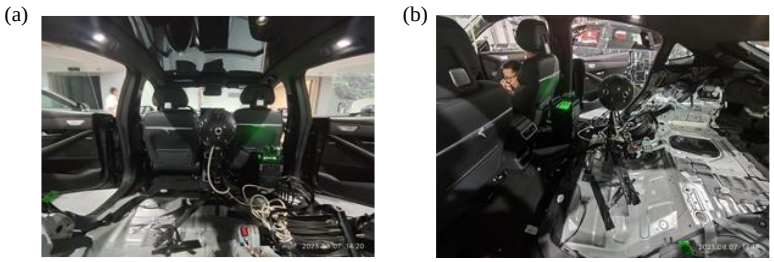

Figure 3. Experimental layout.

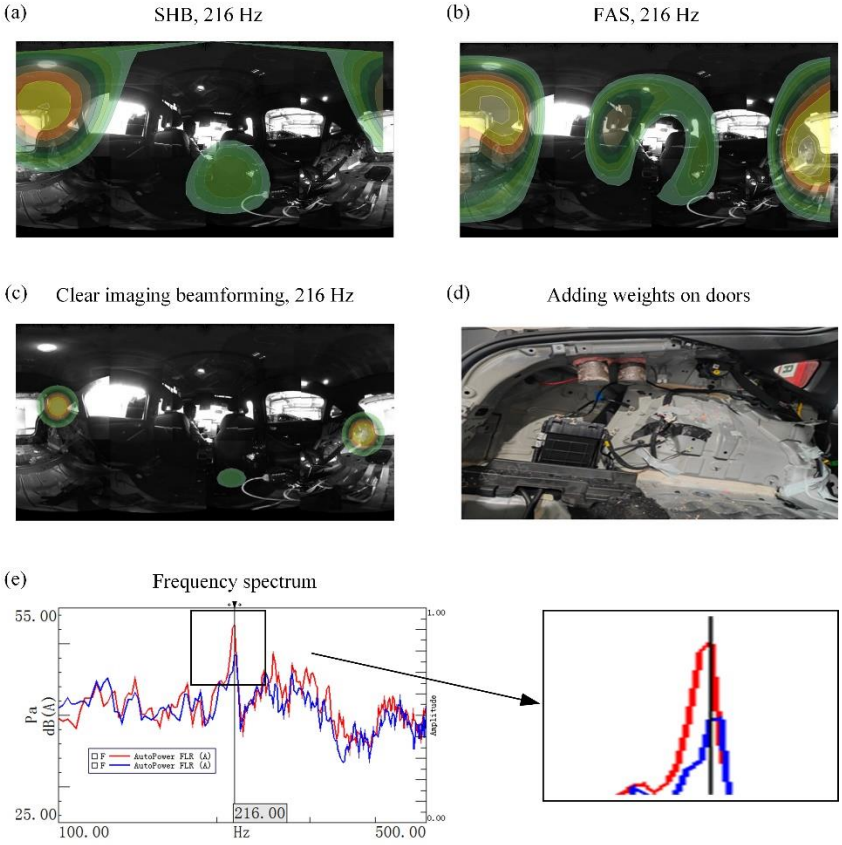

Figure 4. Experimental result. **(a)** SHB, 216Hz; **(b)** FAS, 216Hz; **(c)** Clear imaging beamforming, 216Hz; **(d)** Adding weights on doors; **(e)** Frequency spectrum.

4. Conclusions

To accurately localize the noise sources in car cabin, this paper proposes clear imaging beamforming method, which regards SHB output as a sum of contribution of each incoherent source and repeatedly removes the independent output of each source from SHB output based on coherence between sidelobe and mainlobe to achieve source identification. Through simulations, we could see that compared with SHB and FAS, the proposed method shows much narrower mainlobes, providing sufficiently clear imaging without sacrificing computational efficiency. Furthermore, the proposed method is used to identify noise sources inside a car cabin and the results show that it could effectively indicate the position of noise sources and helps in noise control and sound quality improvement. However, the proposed method cannot identify coherent sources, since it removes the coherent components of the strongest source in each iteration. In our future work, we will focus on the clear imaging beamforming methods applicable to coherent sources.

Author contributions: Writing-original draft, YW and JX; supervision, funding acquisition, YY and ZC; methodology, YW and LY; simulation, YW and JX; validation, LY, JX and ZC; writing-review and editing, YY and ZC. All authors reviewed the results and approved the final version of the manuscript.

Funding: This research was funded by the Open Foundation of the State Key Laboratory of Vehicle NVH and Safety Technology (Grant No. NVHSKL-202202).

Acknowledgements: The authors would like to acknowledge the support from the Open Foundation of the State Key Laboratory of Vehicle NVH and Safety Technology and the facilities provided by Chongqing ChangAn Automobile Co., Ltd. for the experimental research.

Availability of data and materials: The data used to support the findings of this study are available from the corresponding author upon request.

Conflict of interest: The authors declare no conflict of interest.

References

1. Huang L, Sun Z, Yu C, Zhang Y, and Yan B. The Noise exposure of urban rail transit drivers: hazard classification, assessment, and mitigation strategies. Appl. Sci-Basel. 2024, 14(16): 7388. DOI:10.3390/app14167388.
2. Tao Y, Chai Y, Kou L, and Kwan M. Understanding noise exposure, noise annoyance, and psychologocal stress: incorporating individual mobility abd the temporality and the temporality of the exposure-effect relationship. Appl. Geogr. 2021, 125: 102283. DOI: 10.1016/j.apgeog.2020.102283.
3. Wang A, Bista S, Can A, and Chaix B. Personal nise exposure during daily commutes and subjectively reported stress: A trip stage level analysis of mobilisense data. J. Transp. Health 2023, 30: 101612. DOI: 10.1016/j.jth.2023.101612.
4. Battista G, Chiariotti P, and Castellini P. Spherical harmonics decomposition in inverse acoustic methods involving spherical arrays. J. Sound Vib. 2018, 433, 425-460. DOI: 10.1016/j.jsv.2018.05.001.
5. Kreidl H. Increased spatial resolution for sound source location in the automotive industry with the help of new microphone arrays and optimized beamforming algorithms. In Proceedings of the 5th VDI Symposium on Maschinenakustik 2012: Competitive advantage due to low noise products, Karlsruhe, Germany, 13-14 November, 2012.
6. Yin S, Chu Z, Zhang Y and Liu Y. Adaptive reweighting homotopy algorithm based compressive spherical beamforming with spherical microphone arrays. J. Acoust. Soc. Am. 2020, 147(1), 480-489. DOI: 10.1121/10.0000516
7. Wang Y and Chen K. Sound field reconstruction within an entire cavity by plane wave expansion using a spherical microphone array. J. Acoust. Soc. Am. 2017, 142(2), 1858-1870. DOI: 10.1121/1.5006057
8. Haddad, K, and Hald, J. 3D localization of acoustic sources with a spherical array. In Proceedings of the 7th European Conference on Noise Control 2008, Paris, France, 29 June-4 July, 2008.
9. Park M and Rafaely B. Sound field analysis by plane-wave decomposition using spherical microphone array. J. Acoust. Soc. Am. 2005, 118(5), 3094-3103. DOI: 10.1121/1.2063108
10. Meyer J and Elko G. A highly scalable spherical microphone array based on an orthonormal decomposition of the soundfield. In Proceedings of the 2002 IEEE International Conference on Acoustics, Speech and Signal Processing, Orlando, USA, 13-17 May, 2002.
11. Chu Z, Yang Y and He Y. Deconvolution for three-dimensional acoustic source identification based on spherical harmonics beamforming. J. Sound Vib. 2015, 344, 484-502. DOI: 10.1016/j.jsv.2015.01.047.
12. Chu Z, Zhao S, Yang Y and Yang YX. Deconvolution using CLEAN-SC for acoustic source identification with spherical microphone arrays. J. Sound Vib. 2019, 440, 161-173. DOI: 10.1016/j.jsv.2018.10.030.
13. Chu Z, Yin S, Yang Y and Li P. Filter and sum based high resolution CLEAN-SC with spherical microphone arrays. Appl. Acoust. 2021, 182,108278. DOI: 10.1016/j.apacoust.2021.108278.
14. Koretz A and Rafaely B. Dolph-Chebyshev beampattern design for spherical arrays. IEEE Trans. Signal Process. 2009, 57(6), 2417-2420. DOI: 10.1109/TSP.2009.2015120
15. Yan S, Sun H, Svensson P, Ma X and Hoverm J. Optimal modal beamforming for spherical microphone arrays. IEEE-ACM Trans. Audio Speech Lang. 2011, 19(2), 361-371. DOI: 10.1109/TASL.2010.2047815
16. Hald, J. Spherical beamforming with enhanced dynamic range. SAE Int. J. Passeng. Cars Mech. Syst. 2013, 6, 1334-1341. DOI: 10.4271/2013-01-1977
17. Tiana-Roig. E, Torras-Rosell A, Fernandez-Grande. E, Jeong C, Agerkvist F. Enhancing the beamforming map of spherical arrays at low frequencies using acoustic holography. In Proceedings of the 5th Berlin Beamforming Conference 2014, Berlin, Germany, 19-20 February, 2014.